ACS APPLIED MATERIALS & INTERFACES

Research Article

www.acsami.org

Are All-Solid-State Lithium-Ion Batteries Really Safe?—Verification by Differential Scanning Calorimetry with an All-Inclusive Microcell

Takao Inoue and Kazuhiko Mukai*

Toyota Central Research & Development Laboratories, Inc., 41−1 Yokomichi, Nagakute, Aichi 480−1192, Japan

Supporting Information

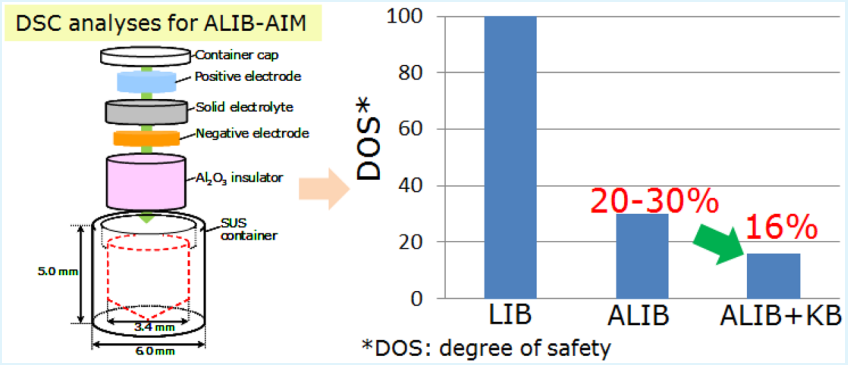

ABSTRACT: Although all-solid-state lithium-ion batteries (ALIBs) have been believed as the ultimate safe battery, their true character has been an enigma so far. In this paper, we developed an all-inclusive-microcell (AIM) for differential scanning calorimetry (DSC) analysis to clarify the degree of safety (DOS) of ALIBs. Here AIM possesses all the battery components to work as a battery by itself, and DOS is determined by the total heat generation ratio (ΔH) of ALIB compared with the conventional LIB. When DOS = 100%, the safety of ALIB is exactly the same as that of LIB; when DOS = 0%, ALIB reaches the ultimate safety. We investigated two types of LIB-AIM and three types of ALIB-AIM. Surprisingly, all the ALIBs exhibit one or two exothermic peaks above 250 °C with 20−30% of DOS. The exothermic peak is attributed to the reaction between the released oxygen from the positive electrode and the Li metal in the negative electrode. Hence, ALIBs are found to be flammable as in the case of LIBs. We also attempted to improve the safety of ALIBs and succeeded in decreasing the DOS down to ∼16% by incorporating Ketjenblack into the positive electrode as an oxygen scavenger. Based on ΔH as a function of voltage window, a safety map for LIBs and ALIBs is proposed.

KEYWORDS: *lithium-ion battery, all-solid-state, nonaqueous electrolyte, solid electrolyte, thermal stability, exothermic reaction*

1. INTRODUCTION

Today's environmental issues, such as emissions of carbon dioxide and global warming, stimulate us to produce cleaner and more efficient electric vehicles (EVs), which are operated by an electrical system and secondary batteries. Since the performance of EVs strongly depends on that of secondary batteries, lithium-ion batteries (LIBs) have received much attention owing to their high energy density and long cycle life.[1,2] The safety of LIBs is, however, a major concern about their application in EVs, because flammable organic solutions are used as an electrolyte.[3]

To overcome such issues, several strategies have been proposed, for instance, replacing organic electrolytes with aqueous electrolytes,[4,5] using additives for a redox shuttle,[6,7] and using separators for an autonomic shutdown.[8,9] Among these strategies, all-solid-state LIBs (ALIBs) using a solid-state Li-ion conductor are regarded as the ultimate solution to improve the battery safety, because of their "nonflammable" character.[10] Nevertheless, to the best of our knowledge, the safety of ALIBs has never been evaluated so far, although current studies on ALIBs are focused on developing solid-state electrolytes with high Li-ion conductivity.[11−13] Thus, the statement that ALIBs are safe remains an attractive hypothesis that should be confirmed.

The best way to investigate the safety of ALIBs (or LIBs) is to monitor ALIBs (or LIBs) under real-use conditions over a long period of time. Such investigation is difficult at present, so thermal abuse tests, such as overcharge and/or nail penetration tests at the fully charged state, are usually employed, particularly for commercial LIBs.[14] These studies provide total information about the safety of LIBs, i.e., cumulative thermal data of all the battery components used in LIBs (positive and negative electrode materials, electrolyte, separator, etc.). In contrast, a differential scanning calorimetry (DSC) analysis offers information on the heat generation by each battery component, leading to understanding of its thermal

Received: October 17, 2016
Accepted: December 19, 2016
Published: December 21, 2016

DOI: 10.1021/acsami.6b13224
ACS Appl. Mater. Interfaces 2017, 9, 1507−1515

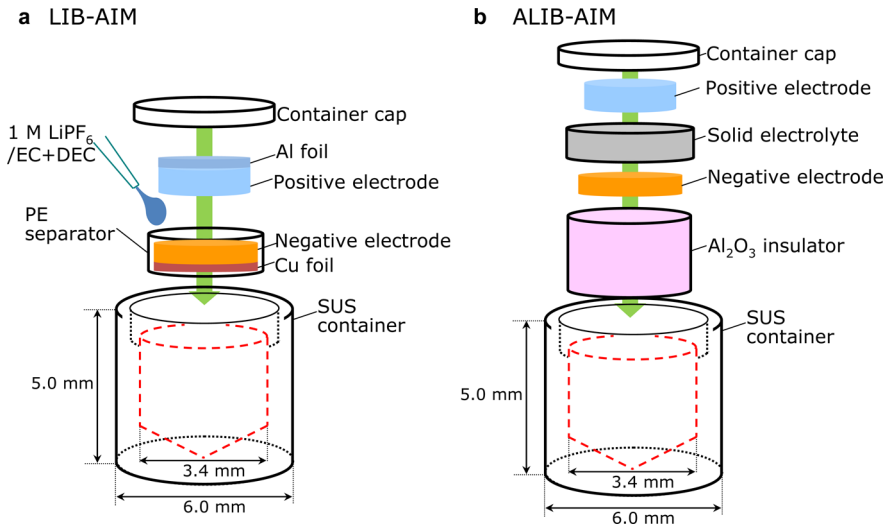

Figure 1. Schematic of procedure of AIM followed for DSC analyses. (a) LIB-AIM; (b) ALIB-AIM. LIB-AIMs consist of all the battery components; positive electrode material, negative electrode material, 1 M $LiPF_6$/EC+DEC (1:1) solution, and current collectors. To avoid an electrical short between the two electrodes, the negative electrode was wrapped in a sheet of PE separator. For ALIB-AIMs, an Al_2O_3 insulator was installed instead of the PE separator. Note that ALIB-AIMs do not contain current collectors; hence, a thermite reaction above ~420 °C occurs only in LIB-AIMs.

stability at elevated temperatures. For example, delithiated Li_xCoO_2 with $x \cong 0.5$, which is widely used as a positive electrode material in commercial LIBs, exhibits two exothermic peaks at around 220 and 250 °C.[15,16]

Here, one inevitably faces a dilemma when examining the safety of ALIBs (or LIBs). The battery safety at elevated temperatures is unveiled for the first time when using all the battery components, but details of each exothermic/endothermic reaction are unclear. Meanwhile, the DSC analysis of each battery component is crucial for understanding of its exothermic/endothermic reactions from changes in enthalpy (ΔH), but the total battery safety is unknown. To cope with this dilemma and to take advantage of both methods, we demonstrate herein an all-inclusive microcell (AIM) constructed in a hermetically sealed pan of the DSC analyses. The AIM is designed to work as a battery by itself. Hence, the AIM not only comprises all the battery components but also possesses an equivalent capacity ratio of positive to negative electrodes as the parent LIB or ALIB.

To verify whether ALIBs are safe and to clarify how safe they are compared with the conventional LIBs, AIMs for both LIB (LIB-AIM) and ALIB (ALIB-AIM) were developed. We first performed the DSC measurements on two different combinations of LIB-AIM up to ~480 °C: one was $LiNi_{0.8}Co_{0.15}Al_{0.05}O_2$ (NCA)|1 M $LiPF_6$ dissolved in ethylene carbonate (EC)/diethyl carbonate (DEC) (1/1 by volume ratio), hereafter denoted as $LiPF_6$ (EC/DEC)|artificial graphite (AG), and the other was $LiNi_{1/3}Co_{1/3}Mn_{1/3}O_2$ (NCM)|$LiPF_6$(EC/DEC)|AG. Combined with the individual DSC data of NCA, NCM, and AG, these studies reveal quantitative contributions of each electrode material as well as total heat generation of the two LIB-AIMs. We then conducted DSC measurements on three different combinations of ALIB-AIM: $LiCoO_2$ (LCO)|garnet-structured $Li_{6.75}La_3Zr_{1.75}Nb_{0.25}O_{12}$ (LLZNO), |Li, LCO|LLZNO|AG, and LCO|LLZNO|$Li[Li_{1/3}Ti_{5/3}]O_4$ (LTO) and compared the results with those of the LIB-AIMs. As a result, we found that AILBs are flammable, as is the case for LIBs and that "the degree of safety (DOS)" is about 30% when compared with that of the conventional LIBs.

2. EXPERIMENTAL SECTION

2.1. Preparation of Electrode Materials. Powder samples of NCA, NCM, LCO, and AG were obtained from Sakai Chemical Industry Co., Ltd., Toda Kogyo, Co., Nippon Chemical Industrial Co., Ltd., and Osaka Gas Chemicals Co., Ltd., respectively. LTO[17] and LLZNO[18] were synthesized by a solid-state reaction technique as reported previously. For LTO, a mixture of $LiOH{\cdot}H_2O$ and TiO_2 anatase powders (Wako Pure Chemical Industries, Ltd.) was well mixed with a pestle and mortar, before heating at 750 °C for 12 h under an oxygen flow.[17] For LLZNO, a mixture of Li_2CO_3, $La(OH)_3$, ZrO_2, and Nb_2O_5 powders (Kojyundo Chemical Lab. Co. Ltd.) was preheated at 950 °C for 12 h in air, crushed into a powder, repressed into a pellet, and finally fired at 1200 °C for 36 h in air.[18] Details of the above syntheses are described elsewhere.[17,18] The crystal structure of NCA, NCM, LCO, AG, LTO, and LLZNO was studied by powder X-ray diffraction (XRD) measurements equipped with Cu Kα radiation (RINT-TTR, Rigaku Co. Ltd.) or Fe Kα radiation (D8 ADVANCE, Bruker AXS, Inc.). Their XRD patterns and lattice parameters are shown in Figure S1.

2.2. Procedure for LIB-AIM. Delithiated or lithiated samples for LIB-AIMs were prepared by an electrochemical reaction. We first constructed a spiral-wound cylindrical LIB with ~750 mAh of capacity using the NCA (or NCM) and AG electrode materials. The electrolyte used was 1 M $LiPF_6$/EC+DEC (1/1) solution for both LIBs. The positive electrode consists of 85 wt % NCA (or NCM), 10 wt % acetylene black (AB), and 5 wt % polyvinylidene fluoride (PVdF) binder. The negative electrode consists of 95 wt % AG and 5 wt % PVdF binder. When preparing the electrodes, a slurry containing the above materials and *N*-methyl-2-pyrrolidone was cast onto an aluminum foil for the positive electrode and onto a copper foil for the negative electrode. The positive and negative electrodes were spirally wound with a polyethylene (PE) separator of 25 μm thickness (Toray Battery Separator Film Co., Ltd.) in a clean room with about −30 °C of a dew point temperature. After transferring to an argon-filled glovebox, ~ 5.0 g (≅ 3.8 mL) of the electrolyte was injected into the LIBs. Each LIB was initially cycled for 5 times at 20 °C for a conditioning. The voltage range was 3.0−4.1 V, and the applied current was 100 mA, which corresponds to ~0.21 mA·cm^{-2} of current density with respect to the surface area of the positive electrode.

For the DSC measurements, each LIB was charged in a constant-current (CC) and constant-voltage (CV) mode up to 4.1 V for a duration of 7 h. The CV charging is needed to homogenize the Li composition in the positive or negative electrode. The charge curves for NCA|$LiPF_6$(EC/DEC)|AG and NCM|$LiPF_6$(EC/DEC)|AG are

DOI: 10.1021/acsami.6b13224
ACS Appl. Mater. Interfaces 2017, 9, 1507−1515

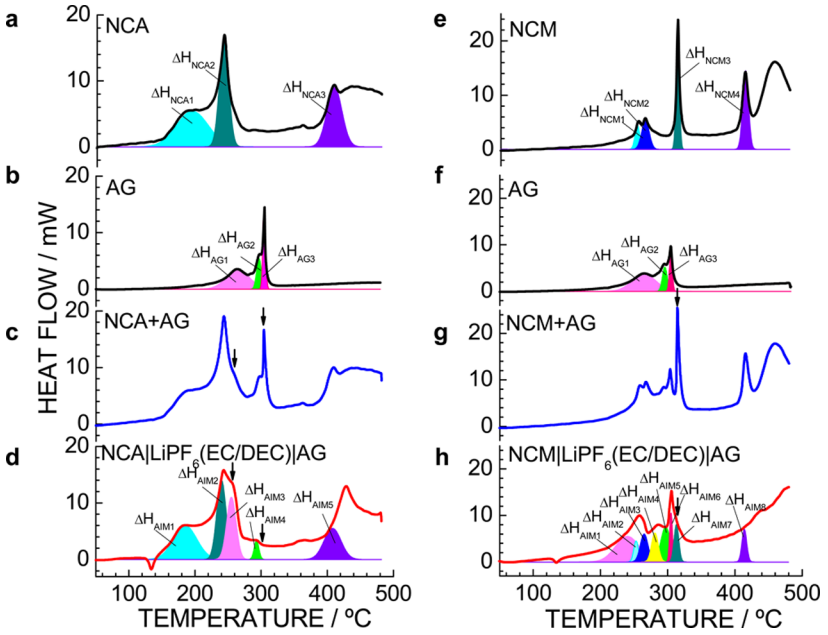

Figure 2. Results of the DSC analyses of LIBs. (a) DSC profile of NCA with the $LiPF_6$(EC/DEC) solution. (b) DSC profile of AG with the $LiPF_6$(EC/DEC) solution (for NCA). (c) Sum of the heat flows in a and b. (d) DSC profile of the LIB-AIM for NCA|$LiPF_6$(EC/DEC)|AG. (e) DSC profile of NCM with the $LiPF_6$(EC/DEC) solution. (f) DSC profile of AG with the $LiPF_6$(EC/DEC) solution (for NCM). (g) Sum of the heat flows in e and f. (h) DSC profile of the LIB-AIM for NCM|$LiPF_6$(EC/DEC)|AG. The arrows in c and d (g and h) indicate the differences in the DSC profiles between the sum of the heat flows of NCA + AG (or NCM + AG) and NCA|$LiPF_6$(EC/DEC)|AG [or NCM|$LiPF_6$(EC/DEC)|AG].

shown in Figure S2. According to the loaded current to the LIBs, x values in $Li_xNi_{0.8}Co_{0.15}Al_{0.05}O_2$ and $Li_xNi_{1/3}Co_{1/3}Mn_{1/3}O_2$ were calculated to be 0.34(1) and 0.39(1), respectively. On the contrary, x values in Li_xC_6 were calculated to be 0.60(1) for NCA|$LiPF_6$(EC/DEC)|AG and 0.57(1) for NCM|$LiPF_6$(EC/DEC)|AG, respectively. The positive and negative electrodes were removed from each LIB in the argon-filled glovebox. Figure 1a shows a schematic of the procedure for LIB-AIM fabrication. We first cut a piece of the electrode from each positive or negative electrode. The weights of the positive and negative electrodes were 3.8 and 1.8 mg, respectively, which correspond to the same weight (capacity) ratio of the positive/negative electrodes in the parent LIB. The negative electrode was then wrapped inside an 8 mm square sheet of the PE separator to electrically insulate it from the positive electrode. After installing the electrodes into the SUS pan for the DSC measurements, 2.3 μL of the electrolyte solution was poured into the LIB-AIM; the amount of electrolyte solution was fixed to 0.52 μL per 1 mg of active material to equalize the conditions of the parent LIB. This is because most of the electrolyte was lost in the separator when deconstructing the LIBs. The dimensions of the SUS pan were of 6 (3.4) mm outside (inside) diameter and 5 mm height. Finally, the SUS pan was hermetically sealed at a pressure of ~370 MPa.

2.3. Procedure for ALIB-AIM. Delithiated and lithiated samples for ALIB-AIM were also prepared by an electrochemical reaction, but the procedure used was different from that used for LIB-AIM. The Li composition in LCO, LTO, and AG was controlled in a half cell with a Li metal electrode. About 80 mg of LCO powder was pressed into a pellet of 1 mm diameter by a uniaxial pressing method with 12 MPa. The LCO pellet, i.e., the electrode without any conducting carbon or binder, was used as a working electrode, and the Li metal was used as a counter electrode. The electrolyte and separator were 1 M $LiPF_6$/EC +DEC (1:1) and 25 μm thick PE membrane, respectively. The fabrication procedure for the LTO/Li and AG/Li cells was essentially the same as that for the LCO/Li cell, but weights of the LTO and AG powders were 40 and 60 mg, respectively.

After fabricating the Li cells in the argon-filled glovebox, the LCO/Li, LTO/Li, and AG/Li cells were charged or discharged to voltages of 4.2, 1.4, and 0.05 V vs Li^+/Li, respectively. This operation was performed in the CC−CV mode for a duration of 100 h. Each working electrode was then removed from the cell and washed with DEC more than 10 times to eliminate the electrolyte existing in the samples. Through assuming that all the loaded current was consumed by the desired electrochemical reactions in each cell, x values in Li_xCoO_2, $Li_{1+x}[Li_{1/3}Ti_{5/3}]O_4$, and Li_xC_6 were calculated to be 0.47(1), 0.98(1), and ~1, respectively. The charge or discharge curves for preparing these samples are shown in Figure S3.

Figure 1b shows a schematic of the procedure for the fabrication of ALIB-AIM. In ALIBs, the solid electrolyte also acts as an insulator. However, simply placing the powder samples of LCO, LTO, and AG together causes an electrical short between the samples. To avoid such electrical shorts, we installed the samples into an Al_2O_3 tube of 3 (2) mm outside diameter and 2 mm height. The weight of the positive electrode (LCO) was 1.2 mg, and that of the negative electrode (LTO, AG, or Li metal) was 1.1 mg. The weight of LLZNO was 15 mg, which seems to be slightly larger than the amount of the solid electrolyte, but is necessary for insulation between the positive and negative electrodes. A current collector such as aluminum foil or copper foil was not used in the ALIB-AIM. The SUS pan was hermetically sealed at a pressure of ~370 MPa, as was the case for the LIB-AIMs.

2.4. DSC Measurements. DSC measurements were performed in the temperature range between room temperature and 480 °C with a heating rate of 5 °C/min (Thermo plus EVO2, DSC8230L, Rigaku Co. Ltd.). To clarify the contribution from each electrode material, we also conducted DSC measurements on each electrode material: NCA with the electrolyte, NCM with the electrolyte, AG with the electrolyte, LCO with or without the electrolyte, LCO with the solid electrolyte, LTO with the solid electrolyte, and AG with the solid electrolyte. The weight of the SUS pan for DSC was checked before and after the DSC measurements to ensure that there were no leakages during the DSC measurements. The weight and number of moles of each material for the DSC measurements are summarized in Table S1. We also performed thermogravimetric (TG) analysis for the LCO ($Li_{0.47}CoO_2$) sample (Thermo plus EVO2, TG8120, Rigaku Co. Ltd.).

3. RESULTS AND DISCUSSION

3.1. DSC Analyses on LIB. To examine the total heat generation in LIBs, we selected NCA, NCM, and AG electrodes

DOI: 10.1021/acsami.6b13224
ACS Appl. Mater. Interfaces 2017, 9, 1507−1515

Table 1. Temperature (T) of Exothermic Peak and Change in Enthalpy (ΔH) for the DSC Analyses of LIBs and ALIBs

battery	composition	T (°C)	ΔH[a]		
			J	J·g^{-1}	kJ·mol^{-1}
LIB	NCA	185 (= ΔH_{NCA1})	5.30	1395	132
		242 (= ΔH_{NCA2})	6.81	1792	169
		410 (= ΔH_{NCA3})	4.24	1116	105
		>410	5.51	1451	137
	AG (for NCA)	256 (= ΔH_{AG1})	2.20	1222	97
		292 (= ΔH_{AG2})	0.85	469	37
		306 (= ΔH_{AG3})	1.11	370	29
	NCA|electrolyte|AG	185 (= ΔH_{AIM1})	4.91	1293p	122p
		240 (= ΔH_{AIM2})	3.78	995p	94p
		254 (= ΔH_{AIM3})	3.53	1963n	155n
		292 (= ΔH_{AIM4})	0.48	270n	21n
		408 (= ΔH_{AIM5})	4.84	1273p	120p
		>410	8.07	2123p	200p
	NCM	254 (= ΔH_{NCM1})	2.14	635	61
		265 (= ΔH_{NCM2})	2.97	880	85
		315 (= ΔH_{NCM3})	4.62	1372	132
		415 (= ΔH_{NCM4})	2.48	736	71
		>415	9.47	2810	271
	AG (for NCM)	265 (= ΔH_{AG1})	2.20	1223	89
		295 (= ΔH_{AG2})	1.09	557	44
		305 (= ΔH_{AG3})	0.68	344	27
	NCM|electrolyte|AG	238 (= ΔH_{AIM1})	4.67	2381n	134n
		257 (= ΔH_{AIM2})	0.84	248p	24p
		266 (= ΔH_{AIM3})	1.04	308p	30p
		281 (= ΔH_{AIM4})	1.48	440p	42p
		296 (= ΔH_{AIM5})	1.05	534n	30n
		305 (= ΔH_{AIM6})	0.41	208n	12n
		315 (= ΔH_{AIM7})	0.77	227p	22p
		415 (= ΔH_{AIM8})	1.25	372p	36p
		>415	14.52	4309p	416p
ALIB	LCO|LLZNO|LTO	256	0.85	610p	57p
	LCO|LLZNO|AG	278	2.04	1455p	137p
	LCO|LLZNO|Li	330, 340	3.96	2200p	207p
	LCO + KB|LLZNO|Li	315	1.01	865p	82p

[a]p denotes ΔH normalized by the weight of the positive electrode material (NCA, NCM, or LCO), whereas n denotes ΔH normalized by the weight of the negative electrode material (AG).

as a model because these materials are currently used for high energy-density LIBs.[1,2] Figure 2 shows the results of the DSC analyses of LIBs, in which panels a–d are for the NCA samples, whereas panels e–h are for the NCM samples. Panel c (or g), denoted as NCA + AG (or NCM + AG), is the simple summation of the DSC profiles for the NCA (or NCM) and AG samples. In the DSC profile shown in Figure 2a, NCA with $LiPF_6$(EC/DEC) exhibits three major exothermic peaks centered around 185, 242, and 410 °C. The ΔH values of the former two exothermic reactions, represented as ΔH_{NCA1} and ΔH_{NCA2}, are calculated to be 1395 (132) and 1792 (169) J·g^{-1} (kJ·mol^{-1}), respectively. ΔH_{NCA1} and ΔH_{NCA2} are attributed to the reaction between oxygen released from the NCA lattice and the EC/DEC solvent, on the basis of previous DSC analyses of NCA:[19,20]

$$Li_xNi_{0.8}Co_{0.15}Al_{0.05}O_2 \rightarrow Li_xNi_{0.8}Co_{0.15}Al_{0.05}O_{2-\delta} + 1/2\delta O_2 \quad (1)$$

and

$$Li_xNi_{0.8}Co_{0.15}Al_{0.05}O_{2-\delta} \rightarrow Ni_{0.8}Co_{0.15}O + 0.025Al_2O_3 + 1/2xLi_2O + (0.4625 - 0.5\delta - 0.25x)O_2 \quad (2)$$

The above two reactions are triggered by the EC/DEC solvent; the onset temperatures of the two exothermic reactions shift to lower temperatures by the presence of the EC/DEC solvent.[20] When the released oxygen reacts with the EC or DEC solvent, the following reaction occurs (in the case of $1/2\delta O_2$):

$$1/5\delta C_3H_4O_3 + 1/2\delta O_2 \rightarrow 3/5\delta CO_2 + 2/5\delta H_2O \quad (3)$$

or

$$1/12\delta C_5H_{10}O_3 + 1/2\delta O_2 \rightarrow 5/12\delta CO_2 + 5/12\delta H_2O \quad (4)$$

The exothermic reaction at 410 °C [ΔH_{NCA3} = 1116 J·g^{-1} (105 kJ·mol^{-1})] has never been reported for NCA. The exothermic reaction above 410 °C [ΔH = 1451 J·g^{-1} (137 kJ·mol^{-1})] is probably due to a thermite reaction[21] because such an exothermic reaction was not observed when the aluminum current collector was removed from the NCA sample. The thermite reaction for NCA is described as

DOI: 10.1021/acsami.6b13224
ACS Appl. Mater. Interfaces 2017, 9, 1507–1515

$$Ni_{0.8}Co_{0.15}O + 2/3Al \rightarrow 0.8Ni + 0.15Co + 1/3Al_2O_3 \quad (5)$$

and its ΔH is calculated to be 3211 J·g^{-1} (303 kJ·mol^{-1}) using the ΔH values for NiO and CoO.[21] As listed in Table 1, the total heat generation in NCA including the thermite reaction is determined to be 21.86 J (543 kJ·mol^{-1}). The ΔH_{NCA} based on the reactions of eqs 1−4 is calculated to be 16.59 J (412 kJ·mol^{-1}), being consistent with the summation of the ΔH_{NCA1}, ΔH_{NCA2}, and ΔH_{NCA3} values [= 16.35 J (406 kJ·mol^{-1})]. In other words, since the maximum temperature for the DSC measurements is limited to ∼480 °C, ∼60% of the thermite reaction between $Ni_{0.8}Co_{0.15}O$ and Al occurs in the temperature above 480 °C.

In the DSC profile of AG with LiPF$_6$(EC/DEC) [Figure 2b], three major exothermic peaks are observed at around 256, 292, and 306 °C, where each ΔH is calculated as 1222 J·g^{-1} (97 kJ·mol^{-1}) for AG1, 469 J·g^{-1} (37 kJ·mol^{-1}) for AG2, and 370 J·g^{-1} (29 kJ·mol^{-1}) for AG3. ΔH_{AG1} is due to the reaction between C_6Li and the LiPF$_6$ salt[22,23]

$$5C_6Li_x + xPF_5 \rightarrow 5C_6 + xP + 5xLiF \quad (6)$$

while ΔH_{AG2} and ΔH_{AG3} are caused by the reaction between C_6Li and the EC/DEC solvent[20,22]

$$4C_6Li_x + xC_3H_4O_3 + xC_5H_{10}O_3 \rightarrow 4C_6 + 2xLi_2CO_3 + 2xC_2H_4 + xC_2H_6 \quad (7)$$

Since the amounts of C_6Li_x and LiPF$_6$ are estimated as 22.8 and 0.79 μmol from the initial preparation, the reactions described in eqs 6 and 7 are limited by the amount of LiPF$_6$ (electrolyte). The observed total heat generation in AG [= 4.16 J (163 kJ·mol^{-1})] is comparable with the calculated ΔH based on the reactions in eqs 6 and 7 [= 3.26 J (142 kJ·mol^{-1})].

One can predict the DSC profile of NCA|LiPF$_6$(EC/DEC)|AG by simply adding up the DSC profiles for the NCA and AG samples. However, as illustrated by the arrows in Figure 2c,d, the DSC profile for NCA + AG is different from that for the actual NCA|LiPF$_6$(EC/DEC)|AG, particularly at around 260−300 °C. In the DSC profile for NCA|LiPF$_6$(EC/DEC)|AG [Figure 2d], five major exothermic peaks are observed at 185, 240, 254, 292, and 408 °C, in which ΔH is 4.91 J for AIM1, 3.78 J for AIM2, 3.53 J for AIM3, 0.48 J for AIM4, and 4.84 J for AIM5. An endothermic peak at around 140 °C is due to the melting reaction of the PE separator. According to the temperatures of ΔH_{AIM}'s, ΔH_{AIM1}, ΔH_{AIM2}, ΔH_{AIM3}, ΔH_{AIM4}, and ΔH_{AIM5} correspond to ΔH_{NCA1}, ΔH_{NCA2}, ΔH_{AG1}, ΔH_{AG2}, and ΔH_{NCA3}, respectively. Hence, these ΔH values are recalculated to be 1293 J·g^{-1} (122 kJ·mol^{-1}), 995 J·g^{-1} (94 kJ·mol^{-1}), 1963 J·g^{-1} (155 kJ·mol^{-1}), 270 J·g^{-1} (21 kJ·mol^{-1}), and 1273 J·g^{-1} (120 kJ·mol^{-1}), respectively, based on the weight of the NCA or AG sample. In contrast to the relative consistency between ΔH_{AIM1} and ΔH_{NCA1} and that between ΔH_{AIM5} and ΔH_{NCA3}, differences are seen in the ΔH values between ΔH_{AIM2} and ΔH_{NCA2}, ΔH_{AIM3} and ΔH_{AG1}, and ΔH_{AIM4} and ΔH_{AG3} (see Table 1). Furthermore, the DSC profile for NCA|LiPF$_6$(EC/DEC)|AG lacks the sharp exothermic peak at around 306 °C, which originated from ΔH_{AG3} in Figure 2b.

For the NCM sample, the difference in the DSC profiles between NCM + AG and NCM|LiPF$_6$(EC/DEC)|AG is also observed, but the situation differs from the NCA case. In the DSC profile shown in Figure 2e, NCM with LiPF$_6$/(EC+DEC) shows four major exothermic peaks centered around 254, 265, 315, and 415 °C, which are denoted as ΔH_{NCM1} [= 635 J·g^{-1} (61 kJ·mol^{-1})], ΔH_{NCM2} [= 880 J·g^{-1} (85 kJ·mol^{-1})], ΔH_{NCM3} [= 1372 J·g^{-1} (132 kJ·mol^{-1})], and ΔH_{NCM4} [= 736 J·g^{-1} (71 kJ·mol^{-1})], respectively. ΔH_{NCM1} and ΔH_{NCM2} correspond to the reaction between oxygen released from the NCM lattice and the EC/DEC solvent, while ΔH_{NCM3} and ΔH_{NCM4} correspond to the combustion reaction of the EC/DEC solvent. The total heat generation including the thermite reaction above 415 °C is determined to be 21.68 J (620 kJ·mol^{-1}). The ΔH of the thermite reaction is calculated to be 2901 J·g^{-1} (280 kJ·mol^{-1}) using following reaction:[21]

$$Ni_{1/3}Co_{1/3}Mn_{1/3}O + 2/3Al \rightarrow 1/3Ni + 1/3Co + 1/3Mn + 1/3Al_2O_3 \quad (8)$$

As seen in Figure 2f, AG with LiPF$_6$/(EC+DEC) shows three major exothermic peaks of ΔH_{AG1} [= 1223 J·g^{-1} (89 kJ·mol^{-1})], ΔH_{AG2} [= 557 J·g^{-1} (44 kJ·mol^{-1})], and ΔH_{AG3} [= 344 J·g^{-1} (27 kJ·mol^{-1})]. These ΔH_{AG} values are slightly lower than those for the case of NCA, due to the different amounts of the electrolyte in the systems. By combining the DSC profiles for the NCM and AG samples, a simple summation DSC profile (NCM + AG) is constructed. However, as clearly shown by the arrows in Figure 2g,h, the DSC profile for NCM + AG is different from that for NCM|LiPF$_6$(EC/DEC)|AG, i.e., the exothermic reaction corresponding to ΔH_{NCM3} (at 330 °C) is missing in the DSC profile for NCM|LiPF$_6$(EC/DEC)|AG. Thus, in the case of the NCM sample, the difference between NCM + AG and LIB-AIM is seen in the positive electrode.

3.2. Origins of the Two Differences. Two differences were observed in the DSC analyses on LIBs: One is the difference between NCA + AG (or NCM + AG) and LIB-AIM, and the other is the difference between NCA and NCM. The former is related to the total amount of the electrolyte in the system. As clearly understood by eqs 1 and 2, the total heat generation in the positive electrode material is limited by the amount of released oxygen, i.e., the amount of delithiated $Li_xNi_{0.8}Co_{0.15}Al_{0.05}O_2$ or $Li_xNi_{1/3}Co_{1/3}Mn_{1/3}O_2$ sample in the system. In contrast, the total heat generation in the negative electrode material (AG) depends on the amount of electrolyte (eqs 6 and 7). Since the amount of electrolyte in AIM-LIB is about two times larger than when the NCA or AG samples were investigated separately (see Table S1), ΔH_{AIM3} in NCA, which is caused by the reaction between C_6Li_x and LiPF$_6$, becomes larger than ΔH_{AG1}. Moreover, the lack of the sharp exothermic peak at around 306 °C in NCA|LiPF$_6$(EC/DEC)|AG is attributed to the depletion of the C_6Li_x; most of the C_6Li_x was consumed in the exothermic reaction of ΔH_{AIM3}. Although we fixed the amount of the LiPF$_6$(EC/DEC) electrolyte as 0.52 μL per 1 mg of active material, further DSC measurements with changing the amount of LiPF$_6$(EC/DEC) could provide more quantitative information on the difference between NCA + AG and LIB-AIM.

The difference between NCA and NCM arises from the difference in the temperature of the phase transition to the rock-salt structure (eq 2).[19,20] The former transforms at around 240 °C, which is lower than the temperature of the reaction between C_6Li_x and LiPF$_6$, whereas the latter transforms at around 310 °C, which is higher than the temperature of the reaction between C_6Li_x and LiPF$_6$. The reason for this difference is attributed to the stabilization of the layered structure by substituting for Ni^{3+} (or Co^{3+}) ions with Mn^{4+}

DOI: 10.1021/acsami.6b13224
ACS Appl. Mater. Interfaces 2017, 9, 1507−1515

ions.[24] For the NCM sample, since the EC/DEC solvent was consumed in the exothermic reactions of ΔH_{AIM3}, ΔH_{AIM4}, ΔH_{AIM5}, and ΔH_{AIM6}, the exothermic reaction due to ΔH_{NCM3} is missing in NCM|LiPF$_6$(EC/DEC)|AG.

As described above, the LIB-AIM method successfully clarified the total heat generation in LIBs as well as the contribution of each exothermic reaction from the positive and negative electrodes. It should be noted that the total heat generation in LIB-AIM for NCA (or NCM) is 25.61 J (or 26.03 J), which is comparable with that in NCA + AG (= 26.02 J) [or NCM + AG (= 25.65 J)] (see Table 1). Thus, the LIB-AIM method also revealed details of the thermal runaway of LIBs, providing a solution for decreasing the total heat generation.

3.3. DSC Analyses on ALIB. The total heat generation in ALIBs was also investigated with the AIM method shown in Figure 1b. We employed LCO and LLZNO as a positive electrode material and solid-state electrolyte, respectively, because these materials are commonly applied in ALIBs due to their high electrical[10,25] or Li^+ ion[10,18] conductivities. In addition, three negative electrode materials of LTO, AG, and Li metal were used to clarify the effect of energy density on the total heat generation. Here LTO is an ideal electrode material for ALIBs, because the change in lattice dimensions is negligibly small during the charge and discharge reactions.[26]

Figure 3a–d shows the DSC profiles for LCO ($Li_{0.47}CoO_2$) with LLZNO, LTO ($Li_{1.95}[Li_{1/3}Ti_{5/3}]O_4$) with LLZNO, AG

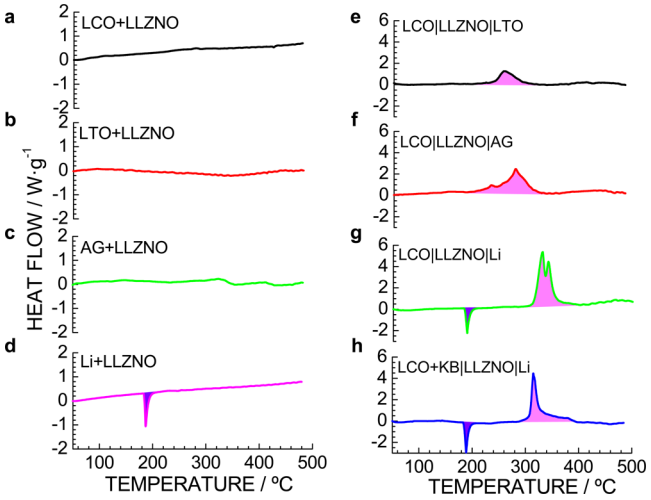

Figure 3. Results of the DSC analyses on ALIBs. (a) DSC profile of $Li_{0.43}CoO_2$ (LCO) with LLZNO. (b) DSC profile of $Li_{1.95}[Li_{1/3}Ti_{5/3}]O_4$ (LTO) with LLZNO. (c) DSC profile of C_6Li (AG) with LLZNO. (d) DSC profile of Li metal with LLZNO. (e) DSC profile of the ALIB-AIM for LCO|LLZNO|LTO. (f) DSC profile of the ALIB-AIM for LCO|LLZNO|AG. (g) DSC profile of the ALIB-AIM for LCO|LLZNO|Li. (h) DSC profile of the ALIB-AIM for LCO + Ketjenblack (KB)|LLZNO|Li. The endothermic peak at around 180 °C is due to the heat of fusion of the Li metal, while the exothermic peaks above 250 °C are attributed to the reaction between the released oxygen from LCO and Li metal.

(C_6Li) with LLZNO, and Li metal with LLZNO, respectively. The values of heat flow ($W \cdot g^{-1}$) are based on the weights of the LCO, LTO, AG, or Li metal sample. Moreover, these DSC profiles correspond to a conventional DSC profile: a delithiated or lithiated electrode material with a liquid electrolyte such as NCA with LiPF$_6$(EC+DEC) [Figure 2a]. For the LCO, LTO, and AG samples shown in Figure 3a–c, neither exothermic nor endothermic peaks are observed up to 480 °C. For the Li metal, however, a sharp endothermic peak is seen at around 185 °C. This endothermic peak is attributed to the heat of fusion of the Li metal and is calculated to be -3.0 kJ·mol^{-1}. Except for the use of the Li metal, these DSC profiles confirm the thermal stability of ALIBs, leading to superior safety performance compared with that of conventional LIBs.

Surprisingly, the DSC profiles for ALIB-AIM shown in Figure 3e–g indicate that there are at least two exothermic peaks above 230 °C. Here, the DSC profiles of LCO|LLZNO|LTO, LCO|LLZNO|AG, and LCO|LLZNO|Li, which are depicted in Figure 3e–g, respectively, correspond to those for NCA|LiPF$_6$(EC/DEC)|AG and NCM|LiPF$_6$(EC/DEC)|AG. The values of heat flow ($W \cdot g^{-1}$) are normalized by the weight of the LCO ($Li_{0.47}CoO_2$) sample. For LCO|LLZNO|LTO, the DSC profile exhibits only one broad exothermic peak centered around 260 °C [$\Delta H_{AIM}^{LTO} = 610$ J·g^{-1} (57 kJ·mol^{-1})]. In the DSC profile for LCO|LLZNO|AG, this exothermic peak is shifted to a slightly higher temperature of ∼280 °C, and the other small exothermic peak is observed at ∼235 °C. The total heat generation in LCO|LLZNO|AG (= ΔH_{AIM}^{AG}) is calculated to be 1455 J·g^{-1} (137.1 kJ·mol^{-1}). For LCO|LLZNO|Li, the DSC profile shows two sharp exothermic peaks at around 330 and 342 °C, together with an endothermic peak due to the fusion of the Li metal at ∼185 °C. The temperatures of these two exothermic peaks are ∼100 °C higher than reported temperatures of LCO with the LiPF$_6$ electrolyte.[16] The heat generation in LCO|LLZNO|Li (= ΔH_{AIM}^{AG}) is calculated to be 2200 J·g^{-1} (207.2 kJ·mol^{-1}) if we ignore the contribution of the heat of fusion of the Li metal.

To clarify the origins of the exothermic peaks in ALIB-LIBs, XRD measurements were performed after the DSC measurements. We first conducted five independent DSC measurements for LCO|LLZNO|Li. We then deconstructed each hermetically sealed SUS pan and collected the three different parts: LCO, LLZNO, and Li metal. Figure S4 shows the XRD patterns of (a) LCO, (b) LLZNO, and (c) the Li metal after the DSC measurements. In the XRD pattern of LCO, Li_xCoO_2, Co_3O_4, and LLZNO phases were observed, while in the XRD pattern of Li metal, Li_2O, Li metal, and LLZNO phases were observed. The lattice parameters of Li_xCoO_2 were calculated to be $a_h = 2.817(1)$ Å and $c_h = 14.032(1)$ Å, indicating that $x \cong 1$. Accordingly, the exothermic peak in LCO|LLZNO|Li can be attributed to the oxidation reaction of the Li metal. That is, in the first step, oxygen was released from the $Li_{0.47}CoO_2$ lattice forming $LiCoO_2$ and Co_3O_4:

$$Li_{0.47}CoO_2 \rightarrow 0.47LiCoO_2 + 0.177Co_3O_4 + 0.176O_2 \quad (9)$$

The released oxygen then reacted with Li metal in the reaction of

$$0.704Li + 0.176O_2 \rightarrow 0.352Li_2O \quad (10)$$

The formation enthalpies (Δ_fH's) of $LiCoO_2$ and $Li_{\sim 0.5}CoO_2$ have been investigated by various methods; i.e., temperature dependence of open circuit voltages,[27] high-temperature oxide melt solution calorimetry,[28] and first-principles calculations.[29] By using Δ_fH of Co_3O_4 (= −910 kJ·mol^{-1}),[30] ΔH of eq 9 is calculated to be 67.98 kJ·mol^{-1} for ref 27, − 138 kJ·mol^{-1} for ref 28, or −4.9 kJ·mol^{-1} for ref 29. Although the calculated ΔH values significantly differ from each other, the reaction of eq 9 can be neglected for the consideration of the heat generation in LCO|LLZNO|Li. This is because DSC analysis on $Li_{0.47}CoO_2$

DOI: 10.1021/acsami.6b13224
ACS Appl. Mater. Interfaces 2017, 9, 1507–1515

not including the $LiPF_6$(EC/DEC) electrolyte revealed no exothermic/endothermic peak up to 450 °C, as shown in Figure S5a. In addition, its TG analysis indicated the formation of Co_3O_4 phase, not CoO[15] phase (see Figure S5b). Since Δ_fH of Li_2O is −598.73 kJ·mol^{-1},[30] ΔH for eq 10 is calculated to be 210.75 kJ·mol^{-1} based on the weight of the LCO sample. The calculated ΔH only for the reaction of eq 10 is very close to the observed ΔH (= 207.2 kJ·mol^{-1}).

The exothermic peaks in LCO|LLZNO|LTO and LCO|LLZNO|AG are also caused by the reaction between the released oxygen and the Li metal, but the situation slightly differs from the case in LCO|LLZNO|Li, because the Li^+ ions are restricted to the LTO or AG lattice. In the cases of LCO|LLZNO|LTO and LCO|LLZNO|AG, Li metal is required to first be removed from the LTO or AG lattice. Δ_fH is reported to be −165 kJ·mol^{-1} for $Li_2[Li_{1/3}Ti_{5/3}]O_4$,[31] while it is −2.3 or −60 kJ·mol^{-1} for AG.[32,33] By subtracting this value from Δ_fH of Li_2O, the ΔH values for LTO and AG are calculated to be 94.59 and 208.65 or 168.13 kJ·mol^{-1}, respectively. The calculated ΔH value for LTO or AG is slightly different from each observed ΔH value: 57 kJ·mol^{-1} for LTO and 137 kJ·mol^{-1} for AG. This deviation mainly comes from an estimation of Δ_fH for $Li_2[Li_{1/3}Ti_{5/3}]O_4$ or C_6Li. In other words, in contrast to $Li_{0.47}CoO_2$, ΔH for LTO or AG strongly depends on the process of the extraction of Li^+ ions from the LTO or AG lattice.

3.4. Comparison between LIBs and ALIBs and Their Safety Map. As evident by the DSC analyses of three types of ALIB-AIM investigated, AILBs also generate heat at elevated temperatures. Since such heat generation can be regarded as a combustion reaction of involving O_2, AILBs are found to be flammable as is the case for LIBs. To clarify the DOS, that is, how much safer ALIBs are compared with LIBs, the temperature dependence of the integral heat flow (ΔH) is shown in Figure S6. We restricted the maximum temperature to 420 °C to avoid the contribution of the thermite reaction. In addition, all the ΔH values are normalized by the weight of the positive electrode material. For LIBs, ΔH at 420 °C is 446 kJ·mol^{-1} for NCA|$LiPF_6$(EC/DEC)|AG and 519 kJ·mol^{-1} for NCM|$LiPF_6$(EC/DEC)|AG. In contrast, ΔH at 420 °C is 57 kJ·mol^{-1} for LCO|LLZNO|LTO, 137 kJ·mol^{-1} for LCO|LLZNO|AG, and 207 kJ·mol^{-1} for LCO|LLZNO|Li. Thus, DOS of ALIB (LCO|LLZNO|AG) is calculated to be 30.7 or 26.4% based on ΔH for NCA|$LiPF_6$(EC/DEC)|AG or NCM|$LiPF_6$(EC/DEC)|AG, respectively. Here when DOS = 100%, the safety of ALIB is equal to that of the corresponding LIB, and when DOS = 0%, ALIB achieves ultimate safety. Although the ΔH_{AIM} value for LCO|$LiPF_6$(EC/DEC)|AG is currently unknown, the simple summation of LCO and AG (LCO + AG) is 480 kJ·mol^{-1} at 420 °C (Figure S7). DOS = 28.5%, if we use this value instead of ΔH_{AIM} for LCO|$LiPF_6$(EC/DEC)|AG.

We attempted to decrease the DOS for the LCO|LLZNO|Li combination, because its energy density is the maximum among the three combinations. Since the released O_2 from LCO brings about heat generation in ALIBs, the DOS is thought to be decreased if we can decrease the amount of O_2. We added 28 wt % of Ketjenblack (KB) into the positive electrode as an O_2 scavenger, expecting the reaction of $C + O_2 \rightarrow CO_2$ (Δ_fH = −393.5 kJ·mol^{-1}) before the reaction of $Li + 1/2O_2 \rightarrow 1/2Li_2O$ (Δ_fH = −598.73 kJ·mol^{-1}). Figure 3h shows the DSC profile for LCO + KB|LLZNO|Li. Although an exothermic peak is observed above 300 °C, ΔH at 420 °C is limited to 79 kJ·mol^{-1}, which corresponds to ∼16% of DOS based on the ΔH for LCO + AG (Figure S6). Thus, as expected, O_2 scavenger additives are effective for decreasing the DOS of ALIB. Note that the amount of KB is about 10 times larger than the calculated KB based on eq 10. Moreover, carbons such as KB and AB are normally used in conventional LIBs to increase the electrical conduction in the electrodes, although current electrodes in ALIBs do not contain conducting carbons.[10−13] Besides decreasing the DOS, incorporating KB into the electrode of ALIBs would provide a positive influence on their rate capability and power performances. This aspect is very important, because overall battery performance is required for the application of ALIBs. In the present study, we simply mixed the KB and LCO powders. Adding a surface coating of carbon on the LCO particles and/or additives for the negative electrode would further decrease the DOS of ALIBs, including the LCO|LLZNO|LTO and LCO|LLZNO|AG combinations. It should be emphasized that the key point is to replace the reaction of $Li + 1/2O_2 \rightarrow 1/2Li_2O$ with a milder exothermic reaction with low Δ_fH.

Using the results we have outlined, we summarize a "safety map" for LIBs (and ALIBs) in Figure 4, which comprises the

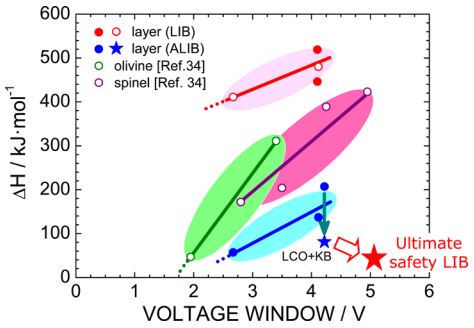

Figure 4. Safety map for LIBs and ALIBs. ΔH is the total heat generation in the DSC analysis up to 420 °C, and voltage window is the difference in operating voltage between the positive and negative electrodes, which corresponds to the energy density of the battery. Although the data for LIB-AIMs (or ALIB-AIMs) with $LiFePO_4$ (olivine), $LiMn_2O_4$ (spinel), and $Li[Ni_{1/2}Mn_{3/2}]O_4$ (spinel) are currently not available, we calculated these ΔH values using the previous DSC analyses in ref 34. According to this safety map, we can evaluate the safety of LIBs or ALIBs in terms of ΔH. Although the mixture of LCO and KB decreases ΔH, present ALIBs still do not reach the ultimate safety LIB with ΔH = 0 kJ·mol^{-1}.

total heat generation (ΔH) and voltage window (V_w) of the battery. Here V_w is the difference in operating voltage between the positive and negative electrodes, which corresponds to the energy density of the battery. Moreover, although the data for LIB-AIMs or ALIB-AIMs with $LiFePO_4$ (olivine), $LiMn_2O_4$ (spinel), and $Li[Ni_{1/2}Mn_{3/2}]O_4$ (spinel), are currently unavailable, we calculated their ΔH values using previously reported DSC analyses.[34] For all the positive electrode materials, ΔH varied almost linearly with V_w, indicating that the battery approaches an unsafe state at elevated temperatures. The slope of ΔH vs V_w depends on the positive electrode material, whereas it seems to be similar between the layered materials, even if we use different electrolytes; $LiPF_6$/(EC+DEC) for LIB and LLZNO for ALIB. The safety of ALIBs is undoubtedly superior to that of LIBs, but DOS is limited to 25−30% regardless of V_w. The combination of LCO and KB decreases to the DOS down to 16%, but it still does not result in the ultimate safety of ALIB with DOS = 0%. To satisfy both high

DOI: 10.1021/acsami.6b13224
ACS Appl. Mater. Interfaces 2017, 9, 1507−1515

energy density and high safety, developments toward the lower right in Figure 4 are encouraged. In addition, further DSC analyses of LIB-AIM and ALIB-AIM with various combinations of a positive electrode material, electrolyte, and negative electrode material are essential to deepen understanding of the thermal stability of LIBs and ALIBs.

As described in the Introduction, the safety of LIBs or ALIBs is evaluated by various thermal abuse tests. Accelerating rate calorimetry (ARC) analysis clarified that the self-heating of LIBs begins at temperature around 90 °C,[35,36] while overcharging of LIBs above ∼5 V induces a rapid increase in temperature up to ∼600 °C.[37] Since ARC is designed to investigate exothermic reactions in an adiabatic condition, a combination of DSC and ARC analyses could provide in-depth insights of thermal stability of LIBs or ALIBs.

4. CONCLUSION

To answer the question of whether or not AILB are ultimately safe, LIB-AIM and ALIB-AIM for the DSC analyses were developed. The answer is unfortunately no, although the total heat generation in ALIBs is ∼30% of that in the conventional LIBs. To face this reality seems to be the only way to reach the ultimate safe battery. We succeeded in decreasing the total heat generation in ALIB down to ∼16%, but we are still in the process of realizing the ultimate safe battery.

■ ASSOCIATED CONTENT

Supporting Information

The Supporting Information is available free of charge on the ACS Publications website at DOI: 10.1021/acsami.6b13224.

XRD patterns of NCA, NCM, LCO, AG, LTO, and LLZNO, charge and discharge curves of NCA and NCM for preparing the AIM samples, charge and discharge curves of LCO, LTO, and AG for preparing the AIM samples, weight and number of moles of each materials for the DSC analyses, XRD patterns after the DSC analyses of LCO, LLZNO, and Li metal, and temperature dependence of ΔH in LIB-AIMs and ALIB-AIMs (PDF)

■ AUTHOR INFORMATION

Corresponding Author

*E-mail: e1089@mosk.tytlabs.co.jp. Phone: +81−561−71−7698. Fax: +81−561−63−6948.

ORCID

Kazuhiko Mukai: 0000-0002-6154-6539

Notes

The authors declare no competing financial interest.

■ ACKNOWLEDGMENTS

We appreciate Tohru Saeki of TCRDL for help with the DSC measurements. We also thank Dr. Shingo Ohta of TCRDL for fruitful discussions on the preparation of ALIB-AIM. K.M. was partially supported by a Grant-in-Aid for Scientific Research (C), 25410207, from the Ministry of Education, Culture, Sports, Science and Technology, Japan.

■ REFERENCES

(1) Dunn, B.; Kamath, H.; Tarascon, J. M. Electrical Energy Storage for the Grid: A Battery of Choices. *Science* **2011**, *334*, 928−935.

(2) Goodenough, J. B.; Park, K.-S. The Li-ion Rechargeable Battery: A Perspective. *J. Am. Chem. Soc.* **2013**, *135*, 1167−1176.

(3) Spotnitz, R.; Franklin, J. Abuse Behavior of High-Power, Lithium-Ion Cells. *J. Power Sources* **2003**, *113*, 81−100.

(4) Li, W.; Dahn, J. R.; Wainwright, D. Rechargeable Lithium Batteries with Aqueous-Electrolytes. *Science* **1994**, *264*, 1115−1118.

(5) Wang, Y.; Yi, J.; Xia, Y. Recent Progress in Aqueous Lithium-Ion Batteries. *Adv. Energy Mater.* **2012**, *2*, 830−840.

(6) Abraham, K. N.; Pasquariello, D. M.; Willstaedt, E. B. n-Butylferrocene for Over-Charge Protection of Secondary Lithium Batteries. *J. Electrochem. Soc.* **1990**, *137*, 1856−1856.

(7) Zhang, L.; Zhang, Z.; Wu, H.; Amine, K. Novel Redox Shuttle Additive for High-Voltage Cathode Materials. *Energy Environ. Sci.* **2011**, *4*, 2858−2862.

(8) Baginska, M.; Blaiszik, B. J.; Merriman, R. J.; Sottos, N. R.; Moore, J. S.; White, S. R. Autonomic Shutdown of Lithium-Ion Batteries using Thermo Responsive Microsperes. *Adv. Energy Mater.* **2012**, *2*, 583−590.

(9) Wu, H.; Zhuo, D.; Kong, D.; Cui, Y. Improving Battery Safety by Early Detection of Internal Shorting with a Bifunctional Separator. *Nat. Commun.* **2014**, *5*, 5193.

(10) Takada, K. Progress and Prospective of Solid-State Lithium Batteries. *Acta Mater.* **2013**, *61*, 759−770.

(11) Kamaya, N.; Homma, K.; Yamakawa, Y.; Hirayama, M.; Kanno, R.; Yonemura, M.; Kamiyama, T.; Kato, Y.; Hama, S.; Kawamoto, K.; Mitsui, A. A Lithium Superionic Conductor. *Nat. Mater.* **2011**, *10*, 682−686.

(12) Kato, Y.; Hori, S.; Saito, T.; Suzuki, K.; Hirayama, M.; Mitsui, A.; Yonemura, M.; Iba, H.; Kanno, R. High-Power All-Solid-State Batteries using Sulfide Superionic Conductors. *Nat. Energ* **2016**, *1*, 16030.

(13) Wang, Y.; Richards, W. D.; Ong, S. P.; Miara, L. J.; Kim, J. C.; Mo, Y.; Ceder, G. Design Principles for Solid-State Lithium Superionic Conductors. *Nat. Mater.* **2015**, *14*, 1026−1031.

(14) For example: *IEC 62133, Secondary Cells and Batteries Containing Alkaline or Other Non-Acid Electrolytes Safety Requirements for Portable Sealed Secondary Cells, and for Batteries Made from Them, for Use in Portable Applications*; International Electrochemical Commission: Geneva, Switzerland, 2012.

(15) MacNeil, D. D.; Dahn, J. R. The Reaction of Charged Cathodes with Nonaqueous Solvents and Electrolytes I. $Li_{0.5}CoO_2$. *J. Electrochem. Soc.* **2001**, *148*, A1205−A1210.

(16) MacNeil, D. D.; Dahn, J. R. The Reactions of $Li_{0.5}CoO_2$ with Nonaqueous Solvents at Elevated Temperatures. *J. Electrochem. Soc.* **2002**, *149*, A912−A919.

(17) Mukai, K.; Nunotani, N.; Moriyasu, R. Relevance between the Bulk Density and Li^+-ion Conductivity in a Porous Eectrolyte: The Case of $Li[Li_{1/3}Ti_{5/3}]O_4$. *ACS Appl. Mater. Interfaces* **2015**, *7*, 20314−20321.

(18) Ohta, S.; Kobayashi, T.; Asaoka, T. High Lithium Ionic Conductivity in the Garnet-Type Oxide $Li_{7-X}La_3(Zr_{2-X}, Nb_X)O_{12}$ (X = 0−2). *J. Power Sources* **2011**, *196*, 3342−3345.

(19) Belharouak, I.; Vissers, D.; Amine, K. Thermal Stability of the $Li(Ni_{0.8}Co_{0.15}Al_{0.05})O_2$ Cathode in the Presence of Cell Components. *J. Electrochem. Soc.* **2006**, *153*, A2030−A2035.

(20) Wang, Y.; Jiang, J.; Dahn, J. R. The Reactivity of Delithiated $Li(Ni_{1/3}Co_{1/3}Mn_{1/3})O_2$, $Li(Ni_{0.8}Co_{0.15}Al_{0.05})O_2$ or $LiCoO_2$ with Non-Aqueous Electrolyte. *Electrochem. Commun.* **2007**, *9*, 2534−2540.

(21) Wagman, D. D.; Evans, W. H.; Parker, V. B.; Schumm, R. H.; Halow, I.; Bailey, S. M.; Churney, K. L.; Nuttall, R. L. *The NBS Tables of Chemical Thermodynamic Properties, Selected Values for Inorganic and C1 and C2 Organic Substance in SI Unites*; American Chemical Society and the American Institute of Physics for the National Bureau of Standards: Washington, D. C., 1982.

(22) Yamaki, J.; Takatsuji, H.; Kawamura, T.; Egashira, M. Thermal stability of graphite anode with electrolyte in lithium-ion cells. *Solid State Ionics* **2002**, *148*, 241−245.

(23) Zhou, M.; Zhao, L.; Okada, S.; Yamaki, J. Quantitative Studies on the Influence of $LiPF_6$ on the Thermal Stability of Graphite with Electrolyte. *J. Electrochem. Soc.* **2012**, *159*, A44−A48.

(24) Yabuuchi, N.; Ohzuku, T. Novel Lithium Insertion Material of $LiCo_{1/3}Ni_{1/3}Mn_{1/3}O_2$ for Advanced Lithium-Ion Batteries. *J. Power Sources* **2003**, *119*−*121*, 171−174.
(25) Ménétrier, M.; Saadoune, I.; Levasseur, S.; Delmas, C. The Insulator-Metal Transition upon Lithium Deintercalation from $LiCoO_2$: Electrode Properties and ^7Li NMR Study. *J. Mater. Chem.* **1999**, *9*, 1135−1140.
(26) Ohzuku, T.; Ueda, A.; Yamamoto, N. Zero-Strain Insertion Material of $Li[Li_{1/3}Ti_{5/3}]O_4$ for Rechargeable Lithium Cells. *J. Electrochem. Soc.* **1995**, *142*, 1431−1435.
(27) Reynier, Y.; Graetz, J.; Swan-Wood, T.; Rez, P.; Yazami, R.; Fultz, B. Entropy of Li Intercalation in Li_xCoO_2. *Phys. Rev. B: Condens. Matter Mater. Phys.* **2004**, *70*, 174304.
(28) Wang, M.; Navrotsky, A.; Venkatraman, S.; Manthiram, A. Entalpy of Formation of Li_xCoO_2 ($0.5 \leq x \leq 1.0$). *J. Electrochem. Soc.* **2005**, *152*, J82−J84.
(29) Wang, L.; Maxisch, T.; Ceder, G. A First-Principles Approach to Studying the Thermal Stability of Oxide Cathode Materials. *Chem. Mater.* **2007**, *19*, 543−552.
(30) NIST-JANAF Thermochemical Tables, 3rd ed.; Chase, M. W., Jr., Davies, C. A., Downey, J. R., Jr., Frurip, D. J., McDonald, R. A., Syverud, A. N., Eds.; *JPCRD 14*, **1985**, Supplement No. 1, pp 1−1856.
(31) Yi, T.-F.; Xie, Y.; Zhu, Y.-R.; Zhu, R.-S.; Shen, H. Structural and Thermodynamic Stability of $Li_4Ti_5O_{12}$ Anode Material for Lithium-Ion Battery. *J. Power Sources* **2013**, *222*, 448−454.
(32) Reynier, Y. F.; Yazami, R.; Fultz, B. Thermodynamics of Lithium Intercalation into Graphites and Disordered Carbons. *J. Electrochem. Soc.* **2004**, *151*, A422−A426.
(33) Avdeev, V. V.; Savchenkova, A. P.; Monyakina, L. A.; Nikol'skaya, I. V.; Khvostov, A. V. Intercalation Reactions and Carbide Formation in Graphite-Lithium System. *J. Phys. Chem. Solids* **1996**, *57*, 947−949.
(34) Xiang, H. F.; Wang, H.; Chen, C. H.; Ge, X. W.; Guo, S.; Sun, J. H.; Hu, W. Q. Thermal Stability of $LiPF_6$-Based Electrolyte and Effect of Contact with Various Delithiated Cathodes of Li-Ion Batteries. *J. Power Sources* **2009**, *191*, 575−581.
(35) Spotnitz, R.; Franklin, J. Abuse Behavior of High-Power, Lithium-Ion Cells. *J. Power Sources* **2003**, *113*, 81−100.
(36) Feng, X.; Fang, M.; He, X.; Ouyang, M.; Lu, L.; Wang, H.; Zhang, M. Thermal Runaway Features of Large Format Prismatic Lithium Ion Battery Using Extended Volume Accelerating Rate Calorimetry. *J. Power Sources* **2014**, *255*, 294−301.
(37) Ouyang, M.; Ren, D.; Lu, L.; Li, J.; Feng, X.; Han, X.; Liu, G. Overcharge-Induced Capacity Fading Analysis for Large Format Lithium-Ion Batteries with $Li_yNi_{1/3}Co_{1/3}Mn_{1/3}O_2$ + $Li_yMn_2O_4$ Composite Cathode. *J. Power Sources* **2015**, *279*, 626−635.

DOI: 10.1021/acsami.6b13224
ACS Appl. Mater. Interfaces 2017, 9, 1507−1515